NASA-CR-191255

TECHNION RESEARCH AND DEVELOPMENT FOUNDATION LTD.

TECHNION CITY, HAIFA 32000, ISRAEL

Annual Report on Research No. 160-573:

Multi-Disciplinary Optimization of Aeroservoelastic System

Sponsored by NASA Grant NAGW-1708

Principal Investigator: Mordechay Karpel, Associate Professor

Faculty of Aerospace Engineering

M. Karpel

Principal Investigator

November 15, 1992

Date

The purpose of the research project "Multi-Disciplinary Optimization of Aeroservoelastic Systems" in its third year (October 1991 to September 1992) was to continue the development of new methods for efficient aeroservoelastic analysis and optimization. The main targets in this year were to complete the development of analytical tools for the investigation of flutter with large stiffness changes, to continue the work on efficient continuous gust response and sensitivity derivatives, and to advance the techniques of calculating dynamic loads with control and unsteady aerodynamic effects.

An efficient and highly accurate mathematical model for time-domain analysis of flutter during which large structural changes occur was developed in cooperation with Carol D. Wieseman of NASA Langley. The model was based on the second-year work "Modal Coordinates for Aeroelastic Analysis with Large Local Structural Variations" recently accepted for publication in the Journal of Aircraft. The flutter time simulation work, "Time Simulation of Flutter with Large Stiffness Changes", was presented by Ms. Wieseman at the 33rd Structures, Structural Dynamics and Materials Conference in Dallas, Texas, April 1992. The paper was also accepted for publication in the Journal of Aircraft.

The work on continuous gust response, together with Arie Zole, a Technion Master student, has been completed. An abstract of the paper "Continuous Gust Response and Sensitivity Derivatives Using State-Space Models" was submitted for presentation in the 33rd Israel Annual Conference on Aviation and Astronautics, February 1993. The abstract is given in Appendix A. A full paper will be shortly submitted for Journal publication. The work extends the optimization model to deal with continuous gust objectives in a way that facilitates their inclusion in the efficient multi-disciplinary optimization scheme.

Currently under development is a works designed to extend the analysis and optimization capabilities to loads and stress considerations. The work, together with Eyal Presente, a Technion Master student, is on aircraft dynamic loads in response to impulsive and non-impulsive excitation. The work extends the formulations of the mode-displacement and summation-of-forces methods to include modes with significant local distortions, and load modes. An abstract of the paper "Structural Dynamic Loads in Response to Impulsive Excitation", submitted for presentation in the International Forum on Aeroelasticity and Structural Dynamics 1993, Strasbourg, France, May 1993, is given in Appendix B.

Another work performed this year under the Grant was "Size-Reduction Techniques for the Determination of Efficient Aeroservoelastic Models" given in Appendix C. The work will be published as a Chapter in Academic Press Volume 54, *"Advances in Control and Dynamic Systems"*.

Appendix A

CONTINUOUS GUST RESPONSE AND SENSITIVITY DERIVATIVES USING STATE-SPACE MODELS

Arie Zole and Mordechay Karpel
Technion-Israel Institute of Technology
Haifa,Israel

INTRODUCTION

An atmospheric flight vehicle is exposed to air turbulence that causes time-varying aerodynamic loads. These continuous-gust loads, amplified by the aeroelastic response of the vehicle, may result in critical structural design conditions. The response of the automatic flight control system to structural vibrations may also play an important role. The gust response is analyzed by aeroservoelastic models which include unsteady aerodynamic, control and structural dynamics effects.

The gusts caused by air turbulence are defined in statistical terms by their power spectral density (PSD) functions and root-mean-square (RMS) values. Aviation regulations define the RMS gust velocity values for which the RMS responses over the entire structure should be analyzed and substantiated. Classical frequency-domain methods[1] are used to calculate the structural response by first calculating the response to sinusoidal gusts, and the associated response PSD at many frequency points. Numerical integration is then used to calculate the RMS response.

Modern aeroservoelastic modeling techniques, which are based on constant-coefficient, time-domain, first-order (state-space) formulation[2], opened the way for a significantly more efficient way to analyze continuous gust response. Augmentation of the aeroelastic states by a gust filter[3], in a way that results in a linear system excited by white noise, facilitated a direct solution for the RMS response. The main difficulty of the state-space modeling is in the requirement for approximating the unsteady aerodynamic force coefficient matrices by rational functions of the Laplace variable. The resulting model contains aerodynamic states which represent the time lag in the development of the aerodynamic forces. The minimum-state method[4] results in a relatively small number of aerodynamic states, which yields efficient aeroservoelastic stability and gust response analyses.

The inclusion of gust response criteria in a simultaneous structural and control design process may be beneficial to the aircraft performance and its structural integrity. The state-space formulation facilitates analytical sensitivity derivatives of gust response parameters with respect to various structural and control design variables. These derivatives allow the efficient inclusion of gust response in the cost function of automated integrated optimization schemes[5] along with other aeroservoelastic criteria such as flutter, control effectiveness and control stability margins.

The purposes of this paper are to apply the minimum-state modeling method to state-space gust response modeling of realistic design cases, to model the gust filter in a way that avoids numerical difficulties, to develop the associated gust response equations, to de-

velop expressions for analytic sensitivity derivatives, and to demonstrate the efficiency and accuracy of the suggested modeling scheme in comparison with classical methods.

KEY EQUATIONS

Modal representation of the structural dynamics, rational approximation of the unsteady aerodynamic coefficients, state-space realization of the control transfer functions and the introduction of a modified gust filter yield the closed-loop state-space equation of motion

$$\{\dot{x}\} = [A]\{x\} + \{B_w\}w \tag{1}$$

where the state vector include generalized structural displacements and velocities, and aerodynamic, control and gust states

$$\{x\}^T = \left[\begin{array}{cccc} \xi & \dot{\xi} & x_a & x_c & x_g \end{array} \right]$$

w represents a white-noise process and $\{B_w\}$ has a single non-zero term in the $\{x_g\}$ row of Eq. (1). Structural response and external loads can be defined by the output equation

$$\{y\} = [C]\{x\} \tag{2}$$

Solution for the state covariance matrix $[X]$ is obtained by solving the Lyapunov equation

$$[A][X] + [X][A]^T = -\{B_w\}\{B_w\}^T \tag{3}$$

The mean square of a response parameter is

$$\sigma_y^2 = [C_y][X][C_y]^T \tag{4}$$

where $[C_y]$ is a row in $[C]$. The computation of the sensitivity derivative of σ_y with respect to a design variable p starts with the definition of $\frac{\partial}{\partial p}[A]$ and $\frac{\partial}{\partial p}[C_y]$ (given in the paper for various structural and control parameters). Differentiation of Lyapunov equation (3) yields a Lyapunov equation for the derivatives of $[X]$.

$$[A]\frac{\partial}{\partial p}[X] + \frac{\partial}{\partial p}[X][A]^T = -\frac{\partial}{\partial p}[A][X] - [X]\frac{\partial}{\partial p}[A]^T \tag{5}$$

Differentiation of Eq. (4) yields

$$\frac{\partial}{\partial p}\sigma_y^2 = [C_y]\frac{\partial}{\partial p}[X][C_y]^T + 2\frac{\partial}{\partial p}[C_y][X][C_y]^T \tag{6}$$

The same Schur decomposition of $[A]$ can be used for all responses and their sensitivity derivatives.

SELECTED RESULTS

The modeling method and the solution process are demonstrated with a twelve-mode model of a transport aircraft at subsonic flight. The aircraft has one control surface and is

exposed to vertical continuous gust. The control system relates the control surface deflection to wing-tip acceleration through a second-order control law and a third-order actuator. The generalized structural properties and the doublet-lattice unsteady aerodynamic data base were calculated using the MSC/NASTRAN finite-element program. Minimum-state aerodynamic approximations were performed using the MIST code[4]. The state-space model has 23 structural states (the heave displacement state is eliminated to avoid a zero root), 4 aerodynamic states, 5 control states and 3 Dryden gust states (with a low-pass filter to avoid a noise term in the output equation).

Open-loop flutter and gust-response results are within 2% of those obtained by frequency-domain methods. The same aerodynamic data base was used for the state-space and frequency-domain solutions. The aerodynamic approximation (not required in the frequency-domain solution) took about 7 cpu seconds on a VAX 9000 machine. One approximation is used for numerous flutter, gust response and sensitivity derivative analyses. State-space cpu times for flutter and a single gust response solution were 0.44 and 0.12 seconds respectively. The cpu time for the respective frequency-domain solutions were about 15 times larger.

The variations of wing-tip acceleration and wing-root bending moment RMS responses with the thickness of an additional plate near the wing root are shown in Figure 1. The expected values are based on sensitivity derivatives. It is clear that the the sensitivity derivatives are accurate. The additional computation time required to calculate a derivative is less than that required to calculate the response itself because both computations are performed with the same matrix decomposition.

It can be concluded that the proposed modeling and solution procedures are suitable for inclusion in efficient automated design procedures with numerous response parameters and design variables (structural and control).

REFERENCES

1. Bisplinghoff,R. L., H. Ashley, and R. L. Halfman, "Aeroelasticity," Addison-Weseley, Cambridge, Mass., 1955.

2. Roger, K. L., "Airplane Math Modeling and Active Aeroelastic Control Design," **AGARD-CP-228**, 4.1-4.11 (1977).

3. Mukhopadhyay, V., J. R. Newsome and I. Abel, "A Method for Obtaining Reduced-Order Control Laws for High-Order Systems Using Optimization Techniques," **NASA TP-1876** (1981).

4. Karpel, M. and Hoadley, S.T., "Physically Weighted Approximations of Unsteady Aerodynamic Forces Using the Minimum-State Method", **NASA TP-3025** (1991).

5. Karpel, M., "Multidisciplinary Optimization of Aeroservoelastic Systems," presented at the Air Force/ NASA Symposium on Multidisciplinary Analysis and Optimization, San Francisco, CA, Sept. 1990.

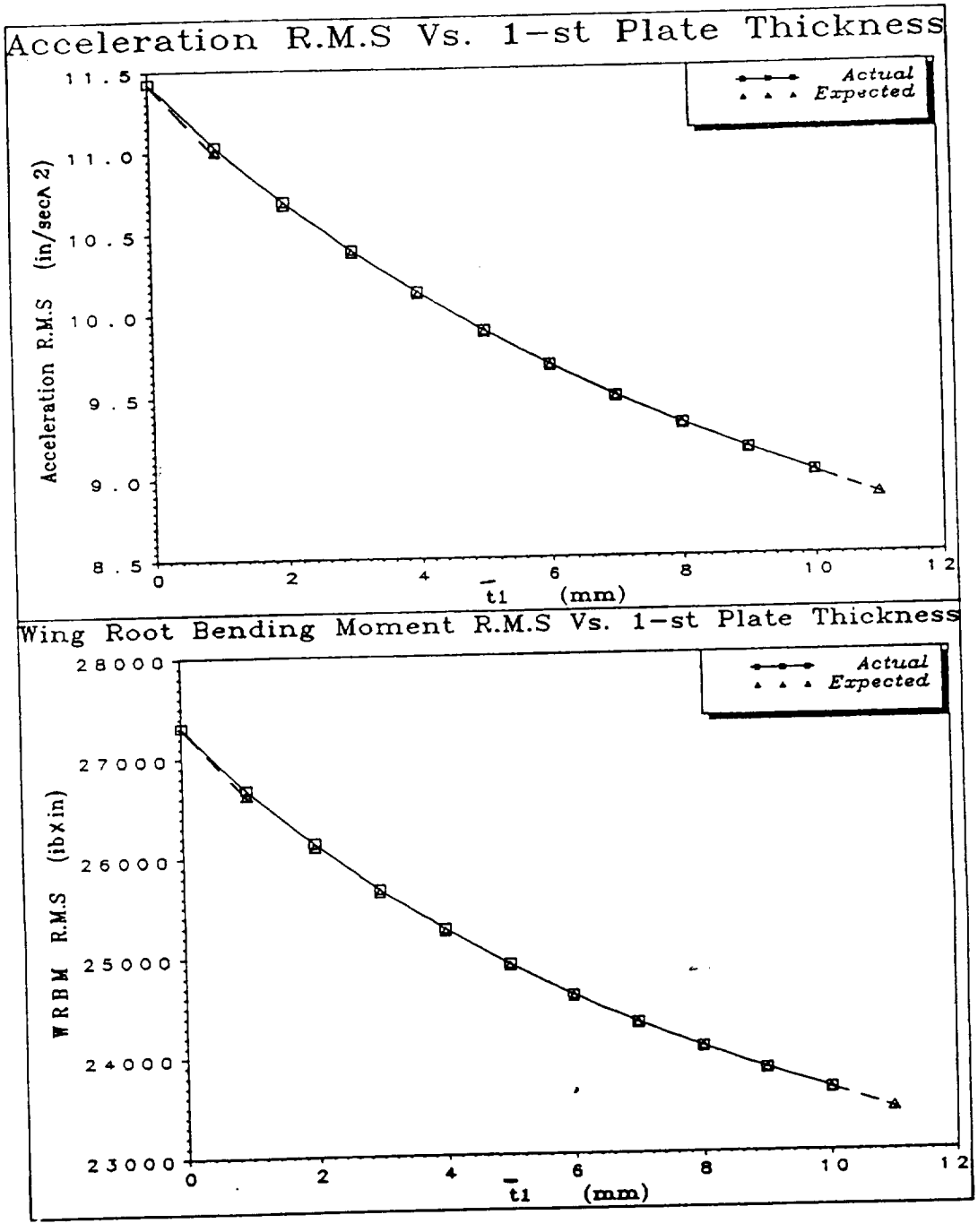
Acceleration R.M.S Vs. 1-st Plate Thickness
Actual
Expected
Acceleration R.M.S (in/sec^2)
11.5
11.0
10.5
10.0
9.5
9.0
8.5
0
2
4
6
8
10
12
t1 (mm)
Wing Root Bending Moment R.M.S Vs. 1-st Plate Thickness
Actual
Expected
WRBM R.M.S (ib×in)
28000
27000
26000
25000
24000
23000
0
2
4
6
8
10
12
t1 (mm)

Figure 1

Appendix B

Structural Dynamic Loads in Response to Impulsive Excitation

Mordechay Karpel and Eyal Presente
Technion - Israel Institute of Technology
Haifa, Israel

The dynamic response of aerospace structures to impulsive excitation such as store ejection and hard landing often yield critical design load cases. Time simulation of the dynamic response is usually based on the modal approach where a subset of low-frequency normal modes serve as generalized coordinates. The dynamic load distributions may be calculated by either the mode-displacement (MD) method, which is based on the generalized displacements, or the summation-of-forces (SOF) method, which sums the inertial, aerodynamic and excitation forces. While MD loads are easier to formulate and analyze , SOF loads are usually more reliable and require a smaller number of modes. The proposed paper presents a comparative investigation of the MD and SOF loads due to local impulsive excitation, and a new method which improves the accuracy and efficiency of the MD analysis dramatically. The new method is based on application of large fictitious masses at the excitation points when the modes are calculated. The fictitious masses cause local distortions which are retained in the modal information when the masses are removed in the response analysis. The local distortions allow local response effects, which are shown to be essential for accurate loads. Fictitious masses are also used to generate artificial load modes which yield simple and efficient expressions for integrated shear forces, bending moments and torsion moments at various wing sections. The time-domain models include unsteady aerodynamic effects which are based on the minimum-state method for rational approximation of the aerodynamic force coefficient matrices. The time simulation is based on analytic expressions.

The methods are demonstrated for store ejection loads on a high aspect ratio wing. Various response cases with and without aerodynamics demonstrate the MD and SOF loads versus number of modes taken into account. Typical 10-mode MD integrated section-load errors without fictitious masses are 10% at wing sections far from the excitation point and 30% at sections close to the excitation point. SOF errors in these cases are about 0.25 of the MD errors. With a single fictitious mass of about one third of the total wing mass loading the excitation point, the 10-mode MD errors are reduced to less than 3% at all the wing sections. SOF errors with fictitious masses are similar to the fictitious-mass MD errors. The new method allows high-accuracy dynamic load computations with the simple MD method which does not require the complicated evaluation of unsteady

Appendix C

SIZE-REDUCTION TECHNIQUES FOR THE DETERMINATION OF EFFICIENT AEROSERVOELASTIC MODELS

Mordechay Karpel

Faculty of Aerospace Engineering
Technion - Israel Institute of Technology
Haifa 32000, Israel

I. INTRODUCTION

Aeroservoelasticity deals with stability and dynamic response of control augmented aeroelastic systems. Flight vehicles are subjected to dynamic loads, such as those caused by atmospheric gusts, which excite the aeroelastic system and cause structural vibrations. The control system senses the vibrations and commands the motion of the control surfaces according to a control transfer function. This closes the aeroservoelastic loop and affects the airframe stability and response characteristics.

The common approach for formulating the equations of motion of an aeroelastic system starts with normal modes analysis of the structural system [1,2]. A realistic, continuous structural system has an infinite number of vibration modes. However, many flutter, structural dynamic response and aircraft performance issues may be adequately analyzed with a limited set of low-frequency vibration modes (including rigid-body modes). Control-surface deflection modes may be added for aeroservoelastic analysis. Complex gust velocity modes may also be added to analyze the response of the structural and control systems to continuous gust.

The unsteady aerodynamic force coefficients are defined with respect to the structural, control-surface and gust modes which serve as generalized

coordinates. The most commonly used unsteady aerodynamic codes, like those based on the Doublet Lattice Method [3], assume that the structure oscillates harmonically. Transcendental unsteady aerodynamic matrices are calculated for various reduced frequency values. Second-order formulations [4] can be used for iterative stability solutions, frequency response, and frequency-domain control synthesis.

The application of various modern control design techniques [5,6], simulation [7] and optimization [8] procedures require the aeroservoelastic equations of motion to be transformed into a first-order, time-domain (state-space) form. This transformation requires the aerodynamic matrices to be approximated by rational functions (ratio of polynomials) in the Laplace domain. The order of the resulting state-space model is a function of the number of selected modes, the number of aerodynamic approximation roots, and the approximation formula. The main considerations in constructing the model are its size (which affects the efficiency of subsequent analyses), its accuracy, and the model construction efforts.

Tiffany and Adams [9] reviewed the most common aerodynamic approximation methods, extended their constraint capabilities and applied them with optimization of the approximation roots. Most methods in [9] are variations of Roger's classic approximation [10] which is based on term-by-term least-square fits. An exception is the Minimum-State (MS) method of Karpel [11, 12] which is based on computationally heavier, iterative, nonlinear least-square solutions, but yields a significant reduction in model size per desired accuracy. Later developments and applications of the MS method [13-16] improved its computational efficiency and introduced a physical weighting algorithm which reduced the number of aerodynamic states required to obtain good accuracy in typical realistic cases to about one fifth of the number of structural states.

A key question that the analyst faces is how many structural modes should be taken into account, and in what manner. The analysis may start with a relatively large number of modes with which the basic aeroservoelastic behavior is studied, such as in [17], and the frequency range of considerable aeroelastic activity is defined. In most applications the analyst selects a number of low-frequency modes to be fully included in the model, and truncates all the modes with higher natural frequency. In many applications, such as control system design, time simulation, parametric studies and structural or control system optimization, it is desired to define a group of modes which are not dominant but may have some effects that should be taken into account. Nissim [18] retained the structural states associated with the less-dominant modes but approximated their aerodynamics with quasi-steady approximations (while the dominant modes are modeled with Roger's approximation), which reduced the number of aerodynamic states. Other applications eliminated the less-dominant modes but used

static residualization techniques, such as in [19], to take into account their steady effects without increasing the model size. This process, which yields accurate results in analysing the rigid-body dynamics, may not be accurate enough in higher frequency flutter mechanisms. Karpel [20] developed a dynamic residualization method in which unsteady effects of the eliminated modes are added to those of the static residualization without increasing the model size.

The purpose of this chapter is to present various size-reduction techniques for the determination of efficient state-space aeroservoelastic models. The frequency-domain equations of motion, which form the basis for the state-space formulation, are reviewed in Section II. Section III develops the aeroservoelastic state-space formulation in general terms. Various aerodynamic approximation techniques are formulated in Section IV using common notations in a way which signifies their differences. The approximation constraints and the least-square solutions are discussed in Section V. The physical weighting algorithm and its use for aerodynamic approximations and for mode selection is described in Section VI. Section VII diescribes the size-reduction techniques which are based on the elimination of structural states. A numerical application which demonstrates and compares the various techniques is given in Section VIII.

II. FREQUENCY-DOMAIN EQUATIONS OF MOTION

The Laplace transform of the open-loop aeroelastic equation of motion in generalized coordinates, excited by control surface motion and atmospheric gusts, is

$$[C_s(s)]\{\xi(s)\} = -\left([M_c]s^2 + q[Q_c(s)]\right)\{\delta(s)\} - \frac{q}{V}[Q_g(s)]\{w_g(s)\} \qquad (1)$$

where

$$[C_s(s)] = [M_s]s^2 + [B_s]s + [K_s] + q[Q_s(s)]$$

where $[M_s]$, $[B_s]$, and $[K_s]$ are the generalized structural mass, damping and stiffness matrices respectively, $[M_c]$ is the coupling mass matrix between the control and the structural modes, $\{\xi\}$ is the vector of generalized structural displacements, $\{\delta\}$ is the vector of control surface commanded deflections, namely the actuator outputs, $\{w_g\}$ is the gust velocity vector, $[Q_s]$, $[Q_c]$ and $[Q_g]$ are the generalised unsteady aerodynamic force coefficient (AFC) matrices associated with the structural, control and gust modes, q is the dynamic pressure and V is the true air speed.

The main difficulty in constructing and solving Eq. (1) is that the AFC matrices are normally not available as an explicit function of s. Common unsteady aerodynamic routines assume that the structure undergoes harmonic oscillations and generate the complex AFC matrices (at a given Mach number) for various values of reduced frequency $k = \omega b/V$ where b is a reference semichord. For open-loop flutter analysis by the $p-k$ method [21], s is replaced in Eq. (1) by pV/b and the roots p_i of $[C_s(p)]$, for which the determinant of $[C_s(p)]$ equals zero, are found iteratively. The AFC matrices $[Q_s(p_i)]$ are approximated by $[Q_s(ik_i)]$, where k_i is the imaginary part of p_i, and are interpolated in each iteration from the tabulated AFC matrices. Flutter conditions are those for which the real part of one of the roots becomes positive (which corresponds to negative damping). Open-loop frequency response to sinusoidal control surface or gust excitation can be calculated by replacing s of Eq. (1) by $i\omega$.

An active control system relates the Laplace transform of the actuator outputs to that of the structural displacements by

$$\{\delta(s)\} = [T(s)][\psi_m]\{\xi(s)\} \qquad (2)$$

where $[T(s)]$ is a matrix of transfer functions relating actuator outputs to sensor inputs, and $[\psi_m]$ is the matrix of modal deflections at sensor inputs. With the assumptions that the pilot does not change the steady control commands and that the actuators are irreversible, the substitution of Eq. (2) into Eq. (1) yields the Laplace transform of the closed-loop equation of motion

$$\left([C_s(s)] + \left[[M_c]s^2 + q[Q_c(s)]\right][T(s)][\psi_m]\right)\{\xi(s)\} = -\frac{q}{V}[Q_g(s)]\{w_g(s)\} \qquad (3)$$

Closed-loop stability and response analyses [4] can be performed similarly to the open-loop analyses, but with $[C_s(s)]$ replaced by the left-side multiplier of $\{\xi(s)\}$ in Eq. (3).

III. STATE-SPACE EQUATIONS OF MOTION

In order to transform Eq. (1) into time-domain constant coefficient equation, the AFC matrices have to be described as rational functions of s. Karpel [11] showed that any rational function approximation of $[Q(s)] = [Q_s\ Q_c\ Q_g]$ that leads to a state-space aeroelastic model can be cast in the form

$$\left[\tilde{Q}(p)\right] = [A_0] + [A_1]p + [A_2]p^2 + [D]\left([I]p - [R]\right)^{-1}[E]p \qquad (4)$$

where p is the nondimensional complex Laplace variable $p = sb/V$ and all the matrix coefficients are real valued. The $[A_i]$ and $[E]$ matrices in Eq. (4) are column partitioned as

$$[A_i] = [A_{s_i}\ A_{c_i}\ A_{g_i}] \quad (i = 0, 1, 2), \qquad [E] = [E_s\ E_c\ E_g] \qquad (5)$$

The gust related columns of $[A_2]$ in Eq. (4) are usually set to $[A_{g_2}] = 0$ to avoid the unnecessary $\ddot{w}_g$ terms in the time-domain model. To facilitate state-space formulation, an augmenting aerodynamic state vector is defined by its Laplace transform as

$$\{x_a(s)\} = \left([I]s - \frac{V}{b}[R]\right)^{-1} \left([E_s]\{\xi(s)\} + [E_c]\{\delta(s)\} + \frac{1}{V}[E_g]\{w_g\}\right) s \tag{6}$$

The resulting state-space open-loop plant equation of motion is

$$\begin{bmatrix} I & 0 & 0 \\ 0 & -\bar{M}_s & 0 \\ 0 & 0 & I \end{bmatrix} \begin{Bmatrix} \dot{\xi} \\ \ddot{\xi} \\ \dot{x}_a \end{Bmatrix} = \begin{bmatrix} 0 & I & 0 \\ \bar{K}_s & \bar{B}_s & \bar{D} \\ 0 & E_s & \bar{R} \end{bmatrix} \begin{Bmatrix} \xi \\ \dot{\xi} \\ x_a \end{Bmatrix} + \\ + \begin{bmatrix} 0 & 0 & 0 \\ \bar{K}_c & \bar{B}_c & \bar{M}_c \\ 0 & E_c & 0 \end{bmatrix} \begin{Bmatrix} \delta \\ \dot{\delta} \\ \ddot{\delta} \end{Bmatrix} + \begin{bmatrix} 0 & 0 \\ \bar{K}_g & \bar{B}_g \\ 0 & \bar{E}_g \end{bmatrix} \begin{Bmatrix} w_g \\ \dot{w}_g \end{Bmatrix} \tag{7}$$

where

$$[\bar{M}_s] = [M_s] + \frac{qb^2}{V^2}[A_{s_2}], \quad [\bar{K}_s] = [K_s] + q[A_{s_0}], \quad [\bar{B}_s] = [B_s] + \frac{qb}{V}[A_{s_1}],$$

$$[\bar{M}_c] = [M_c] + \frac{qb^2}{V^2}[A_{c_2}], \quad [\bar{K}_c] = q[A_{c_0}], \quad [\bar{B}_c] = \frac{qb}{V}[A_{c_1}], \quad [\bar{D}] = q[D],$$

$$[\bar{R}] = \frac{V}{b}[R], \quad [\bar{K}_g] = q[A_{g_0}], \quad [\bar{B}_g] = \frac{qb}{V}[A_{g_1}], \quad [\bar{E}_g] = \frac{1}{V}[E_g]$$

The resulting number of aerodynamic augmenting states in $\{x_a\}$ is the order (n_a) of the aerodynamic lag matrix $[R]$.

It is assumed in this work that the control system, including the actuator dynamics, can be expressed in a state-space form as

$$\begin{aligned} \{\dot{x}_c\} &= [A_c]\{x_c\} + [B_c]\{u\} \\ \begin{Bmatrix} \delta \\ \dot{\delta} \\ \ddot{\delta} \end{Bmatrix} &= \begin{bmatrix} C_{c_0} \\ C_{c_1} \\ C_{c_2} \end{bmatrix} \{x_c\} \end{aligned} \tag{8}$$

where $\{x_c\}$ is the control state vector and $\{u\}$ is the control system input vector. It is also assumed that a gust filter can be defined in the state form

$$\begin{aligned} \{\dot{x}_g\} &= [A_g]\{x_g\} + \{B_g\}w \\ \begin{Bmatrix} w_g \\ \dot{w}_g \end{Bmatrix} &= \begin{bmatrix} C_{g_0} \\ C_{g_1} \end{bmatrix} \{x_g\} \end{aligned} \tag{9}$$

such that the power spectral density functions of the gust velocities in $\{w_g\}$ are obtained when w represents a white-noise process. It should be noted that, unlike in Ref. [20], the output equation in (9) does not contain a w term in its right side. This may require additional gust filter states, but it allows the acceleration measurements below to be formulated without a white-noise term.

Equations (7-9) combine for the open-loop state-space aeroservoelastic equation of motion

$$\begin{bmatrix} I & 0 & 0 & 0 & 0 \\ 0 & -\bar{M}_s & 0 & 0 & 0 \\ 0 & 0 & I & 0 & 0 \\ 0 & 0 & 0 & I & 0 \\ 0 & 0 & 0 & 0 & I \end{bmatrix} \begin{Bmatrix} \dot{\xi} \\ \ddot{\xi} \\ \dot{x}_a \\ \dot{x}_c \\ \dot{x}_g \end{Bmatrix} =$$

$$\begin{bmatrix} 0 & I & 0 & 0 & 0 \\ \bar{K}_s & \bar{B}_s & \bar{D} & \bar{F}_c & \bar{F}_g \\ 0 & E_s & \bar{R} & \hat{E}_c & \hat{E}_g \\ 0 & 0 & 0 & A_c & 0 \\ 0 & 0 & 0 & 0 & A_g \end{bmatrix} \begin{Bmatrix} \xi \\ \dot{\xi} \\ x_a \\ x_c \\ x_g \end{Bmatrix} + \begin{bmatrix} 0 \\ 0 \\ 0 \\ B_c \\ 0 \end{bmatrix} \{u\} + \begin{Bmatrix} 0 \\ 0 \\ 0 \\ 0 \\ B_g \end{Bmatrix} w \tag{10}$$

where

$$\begin{aligned} \left[\hat{E}_c\right] &= [E_c][C_{c_1}] \\ \left[\hat{E}_g\right] &= [\bar{E}_g][C_{g_1}] \\ [\bar{F}_c] &= [\bar{K}_c][C_{c_0}] + [\bar{B}_c][C_{c_1}] + [\bar{M}_c][C_{c_2}] \\ [\bar{F}_g] &= [\bar{K}_g][C_{g_0}] + [\bar{B}_g][C_{g_1}] \end{aligned}$$

or

$$[Z]\{\dot{x}\} = [A]\{x\} + [B]\{u\} + \{B_w\}w \tag{11}$$

where the matrices and vectors correspond to the respective ones in Eq. (10). Outputs of the aeroservoelastic system are expressed in the form

$$\{y\} = [C]\{x\} \tag{12}$$

Structural outputs are based on the matrix $[\psi_m]$ of modal deflections and rotations. Displacements are expressed with $[C] = [\psi_m \ 0 \ 0 \ 0 \ 0]$, velocities with $[C] = [0 \ \psi_m \ 0 \ 0 \ 0]$ and accelerations with

$$[C] = -[\psi_m][\bar{M}_s]^{-1} \begin{bmatrix} \bar{K}_s & \bar{B}_s & \bar{D} & \bar{F}_c & \bar{F}_g \end{bmatrix} \tag{13}$$

Equation (12) can be used to augment Eq. (11) by sensor models. The system outputs in this case would be based on the sensor states. Whether

sensor dynamics are included or ignored, the aeroservoelastic loop is closed by relating the control inputs to system outputs by

$$\{u\} = [G_c]\{y\} \tag{14}$$

where $[G_c]$ is the control gain matrix. The substitution of Eq. (14) into Eq. (10) yields the closed-loop equation of motion

$$[Z]\{\dot{x}\} = [\bar{A}]\{x\} + \{B_w\}w \tag{15}$$

where

$$[\bar{A}] = [A] + [B][G_c][C]$$

It can be noticed from Eq. (10) that only the fourth row of $[\bar{A}]$ is different than that of $[A]$. A $\{u\}$ term can be left in the right side of Eq. (15) to reflect pilot commands.

IV. RATIONAL FUNCTION APPROXIMATIONS

The most commonly used rational function approximations of the AFC matrices are reviewed in this section with emphasis on the resulting number of aerodynamic augmenting states. The approximations are formulated here in the matrix form of Eq. (4), from which their effects on the subsequent state-space model, Eq. (10), can be deduced. All the approximation processes described herein start with the definition of a rational function of the imaginary part (ik) of the nondimensional Laplace variable p. Least-square procedures are then used to calculate the approximation coefficients that best fit the tabulated $[Q(ik_\ell)]$ matrices. The approximation is then expanded to the entire Laplace domain by replacing ik with sb/V. The least-square solution procedures are discussed in Section V.

The Minimum-State (MS) method [11,12] uses the most general expression of Eq. (4) which, with p replaced by ik, is

$$\left[\tilde{Q}(ik)\right] = [A_0] + ik[A_1] - k^2[A_2] + ik[D]\,(ik[I] - [R])^{-1}[E] \tag{16}$$

The MS procedure assumes that $[R]$ is diagonal with n_L distinct negative values. The number of the resulting aerodynamic states in Eq. (10) is $n_a = n_L$. By allowing all the other terms in the coefficient matrices of Eq. (16) to be variables in the fit process, the MS method involves a relatively complicated least-square solution, but it yields a minimal number of aerodynamic states per desired accuracy.

Roger [10] approximated each aerodynamic term separately but with common aerodynamic lags,

$$\left[\tilde{Q}(ik)\right] = [A_0] + ik[A_1] - k^2[A_2] + \sum_{l=1}^{n_L} \frac{ik}{ik + \gamma_l}[A_{l+2}] \tag{17}$$

which can be cast in the form of Eq. (16) with

$$[D] = \begin{bmatrix} I & I & \cdots \end{bmatrix},\quad [R] = -\begin{bmatrix} \gamma_1 I & & \\ & \gamma_2 I & \\ & & \ddots \end{bmatrix},\quad [E] = \begin{bmatrix} A_3 \\ A_4 \\ \vdots \end{bmatrix} \tag{18}$$

The resulting number of aerodynamic states is $n_a = n_L \times n_m$ where n_m is the number of vibration modes.

The Modified Matrix Padé (MMP) method [9] applies Eq. (17) to each column separately

$$\left\{\tilde{Q}(ik)\right\}_j = \{A_0\}_j + ik\{A_1\}_j - k^2\{A_2\}_j + \sum_{l=1}^{n_{L_j}} \frac{ik}{ik + \gamma_{l_j}}\{A_{l+2}\}_j \tag{19}$$

where the number of lags and their values can be different for different columns, which can lead to a lower number of states. When the number of lags (but not their values) are equal, Eq. (19) can be cast in the form of Eq. (16) with

$$[D] = \begin{bmatrix} A_3 & A_4 & \cdots \end{bmatrix},\quad [R] = \begin{bmatrix} R_1 & & \\ & R_2 & \\ & & \ddots \end{bmatrix},\quad [E] = \begin{bmatrix} I \\ I \\ \vdots \end{bmatrix} \tag{20}$$

where

$$[R]_l = -\begin{bmatrix} \gamma_{l_1} & & \\ & \gamma_{l_2} & \\ & & \ddots \end{bmatrix}$$

which is also an alternative representation of Roger's approximation but it yields a larger number of aerodynamic states, $n_a = (n_m + n_c + n_g) \times n_L$ where n_c and n_g are the number of control and gust modes respectively. However, for each $n_{L_j} < n_{l_j} \leq n_L$, the $j + (n_m + n_c + n_g) \times (l-1)$ column in $[D]$ and $[R]$, and the $j + (n_m + n_c + n_g) \times (l-1)$ row in $[E]$ and $[R]$ are eliminated. The resulting number of aerodynamic states is $n_a = \sum n_{L_j}$. It should be noticed that some n_{L_j} values can be zero, which corresponds to quasi-steady aerodynamics and does not add aerodynamic states.

Several studies [9,11-16] compared the aeroelastic models resulting from the MS, Roger and MMP approximations. The number of aerodynamic states, n_a, in the MS models were about 75% smaller than those of the Roger's models with similar accuracy, and $40 - 70\%$ smaller than those of the MMP models. On the other hand, the consideration of both $[D]$ and $[E]$ as free-coefficient matrices in the MS method makes the MS solution more complicated than the others.

Nissim [18] suggested that, with some insight, many aeroelastic problems can be modeled with quasi-steady approximation for most vibration modes. Nissim partitioned the AFC matrices and approximated $[Q_{s_{11}}]$, $[Q_{c_1}]$ and $[Q_{g_1}]$ with Roger's approximation of Eq.(17), and $[Q_{s_{12}}]$, $[Q_{s_{21}}]$, $[Q_{s_{22}}]$, $[Q_{c_2}]$ and $[Q_{g_2}]$ with no lag terms, where subscript 1 relates to structural modes with significant influences on flutter (group one), and 2 relates to the other modes (group two). This approximation can be first cast in the form of Eq. (16) with $[D]$, $[E]$ and $[R]$ of Eq. (18), and then reduced by eliminating the columns in $[D]$ and $[R]$ and the rows in $[R]$ and $[E]$ which are associated with group two. The resulting number of aerodynamic states is $n_a = n_L \times n_{m_1}$, which is demonstrated in [18] to be significantly lower than that of the full Roger's approximation, with a minor loss of accuracy in flutter results. It may be noticed that after the row elimination, the columns of $[E]$ in Eq. (18) associated with group two are zero, which indicates that the $[Q_{s_{12}}]$ partition could be approximated as well by Roger's formula without causing an increase of n_a.

Eversman and Tewari [22] extended Roger's formulation to allow multiple aerodynamic poles. Their baseline distinct-pole approximation is different than Eq. (17) by having one instead of ik in the numerators of the lag terms. Since they both have the same order of numerator polynomials when brought to common denominators, it can be shown that the two approximations are equivalent. The disadvantage in the baseline approximation in [22] is that its $[A_0]$ term does not represent steady aerodynamics as in all the other formulations above. The extended multiple-pole approximation, however, may improve the lag optimization process discussed in the next section.

V. APPROXIMATION PROCEDURES

To facilitate real-valued algebra, the complex approximation expression of Eq. (16) is separated into real and imaginary parts,

$$Re[\tilde{Q}(ik)] \equiv [\tilde{F}(k)] = [A_0] - k^2[A_2] + k^2[D]\left(k^2[I] + [R]^2\right)^{-1}[E] \qquad (21)$$

and

$$Im[\tilde{Q}(ik)] \equiv [\tilde{G}(k)] = k[A_1] - k[D]\left(k^2[I] + [R]^2\right)^{-1}[R][E] \qquad (22)$$

The comparison of Eqs. (21) and (22) with the real and imaginary parts, $[F(k_\ell)]$ and $[G(k_\ell)]$, of the tabulated AFC matrices $[Q(ik_\ell)]$ provides an overdetermined set of approximate equations. The task is to find the free approximation coefficients that minimize, under some constraints, the total least-square approximation error

$$\varepsilon_t = \sqrt{\sum_{i,j,\ell} |\tilde{Q}_{ij}(ik_\ell) - Q_{ij}(ik_\ell)|^2 W_{ij\ell}^2} \qquad (23)$$

where $W_{ij\ell}$ is the weight assigned to the ijth term of the ℓth tabulated AFC matrix. All the procedures associated with the methods presented in Section IV start with an initial set of aerodynamic lags which define $[R]$. The denominator coefficients are then calculated by a sequence of least-square solutions. Some procedures [9, 11, 16, 22] then apply an optimization scheme to modify the lags and repeat the solution for a better fit, until convergence occurs.

The sequence of least-square solutions in each method depends on the formulation and the way constraints and weighting functions are applied. Each individual solution in the sequence is based on the general approximate equation

$$[W^*]_\ell [A^*]_\ell \{x^*\} \approx [W^*]_\ell \{b^*\}_\ell \qquad for\ \ell = 1, n_k \qquad (24)$$

where n_k is the number of tabulated AFC matrices, $\{b^*\}_\ell$ is based on the tabulated data, $[W^*]_\ell$ is a diagonal matrix of weights associated with the terms of $\{b^*\}_\ell$, $\{x^*\}$ is a subset of unknown coefficients which are uncoupled with others, and $[A^*]_\ell$ is a function of k_ℓ, the aerodynamic lag values and the constraints associated with the unknowns. The weighted least-square solution for $\{x^*\}$ is obtained by solving

$$\left(\sum_\ell [A^*]_\ell^T [W^*]_\ell^2 [A^*]_\ell\right)\{x^*\} = \sum_\ell [A^*]_\ell^T [W^*]_\ell^2 \{b^*\}_\ell \qquad (25)$$

The contents of $[A^*]_\ell$, $\{x^*\}$ and $\{b^*\}_\ell$ in the various approximation methods, and the number of least-square solutions in each case, are given in the remaining of this section. For the sake of simplicity, a uniform weighting, $[W^*]_\ell = [I]$, is assumed. Weighting methods are discussed in Section VI. It should be noted that the least-square solutions are not necessarily solved one by one. The solutions for different $\{x^*\}$ vectors that have the same coefficient matrix, in the right side of Eq. (25), can be grouped together to reduce the computational cost.

A. The Unconstrained Problem

In all the approximation methods of Section VI, except the MS method, either $[D]$ or $[E]$ of Eqs. (21) and (22) are constant, which yields a linear least-square problem for a given set of aerodynamic lags. Furthermore, the structure of Eqs. (17) and (19) indicates that the solution in these

cases can be performed for each aerodynamic term separately by performing $n_m \times (n_m + n_c + n_g)$ solutions of Eq. (25) with

$$[A^*]_\ell = \begin{bmatrix} 1 & 0 & -k_\ell^2 & \frac{k_\ell^2}{k_\ell^2+\gamma_{1_j}^2} & \frac{k_\ell^2}{k_\ell^2+\gamma_{2_j}^2} & \cdots \\ 0 & k_\ell & 0 & \frac{k_\ell\gamma_{1_j}}{k_\ell^2+\gamma_{1_j}^2} & \frac{k_\ell\gamma_{2_j}}{k_\ell^2+\gamma_{2_j}^2} & \cdots \end{bmatrix},$$

$$\{x^*\} = \begin{Bmatrix} A_{0_{ij}} \\ A_{1_{ij}} \\ \vdots \end{Bmatrix}, \qquad \{b^*\}_\ell = \begin{Bmatrix} F_{ij}(k_\ell) \\ G_{ij}(k_\ell) \end{Bmatrix} \tag{26}$$

where the number of unknowns in each solution is $n_{L_j} + 3$ in the MMP approximation, Eq. (19), $n_L + 3$ in Roger's approximation, Eq.(17), and either $n_L + 3$ or 3 in Nissim's approximation.

With both $[D]$ and $[E]$ in Eqs. (21) and (22) being unknown, the MS problem for a given $[R]$ is nonlinear. The unconstrained problem is solved iteratively by starting with an initial guess of $[D]$ in which at least one term in each row and each column is nonsero. The unknown matrices $[A_0]$, $[A_1]$, $[A_2]$ and $[E]$ are then calculated by performing $n_m + n_c + n_g$ column-by-column solutions of Eq.(25) with

$$[A^*]_\ell = \begin{bmatrix} I & 0 & -k_\ell^2 I & k_\ell^2[D]\left(k_\ell^2[I]+[R]^2\right)^{-1} \\ 0 & k_\ell I & 0 & -k_\ell[D]\left(k_\ell^2[I]+[R]^2\right)^{-1}[R] \end{bmatrix},$$

$$\{x^*\} = \begin{Bmatrix} A_{0_j} \\ A_{1_j} \\ A_{2_j} \\ E_j \end{Bmatrix}, \qquad \{b^*\}_\ell = \begin{Bmatrix} F_j(k_\ell) \\ G_j(k_\ell) \end{Bmatrix} \tag{27}$$

where the j indices relate to the jth columns of the respective matrices and where the number of unknowns in each solution is $3n_m + n_L$. The calculated $[E]$ is then used to recalculate $[A_0]$, $[A_1]$, $[A_2]$ and $[D]$ by performing n_m row-by-row solutions of Eq.(25) with

$$[A^*]_\ell = \begin{bmatrix} I & 0 & -k_\ell^2 I & k_\ell^2[E]^T\left(k_\ell^2[I]+[R]^2\right)^{-1} \\ 0 & k_\ell I & 0 & -k_\ell[E]^T\left(k_\ell^2[I]+[R]^2\right)^{-1}[R] \end{bmatrix},$$

$$\{x^*\} = \begin{Bmatrix} A_{0_i}^T \\ A_{1_i}^T \\ A_{2_i}^T \\ D_i^T \end{Bmatrix}, \qquad \{b^*\}_\ell = \begin{Bmatrix} F_i^T(k_\ell) \\ G_i^T(k_\ell) \end{Bmatrix} \tag{28}$$

where the i indices relate to the ith rows of the respective matrices and where the number of unknowns in each solution is $3(n_m + n_c + n_g) + n_L$.

Ref. [9] solves the unconstrained problem by repeating the $[D] \rightarrow [E] \rightarrow [D]$ iterations of Eqs. (27) and (28) until convergence is obtained or until the specified maximum number of iterations is reached. Ref. [13] demonstrated that the convergence process does not strongly depend on the initial guess of $[D]$. Theoretically, each iteration reduces the total approximation error defined in Eq. (23). It should be noted, however, that numerical ill-conditioning problems may occur [13,15] when too many aerodynamic lag terms are used. It is therefore recommended that the number of structural modes (n_m) is the upper limit on the number of lags (n_L). This upper limit (which yields the same number of aerodynamic states as Roger's approximation with one lag) is usually more than sufficient to obtain a good aerodynamic fit [11-16, 23].

The iterative nature of the MS procedure and the relatively large number of unknowns solved for simultaneously in each iteration of the unconstrained problem, Eqs. (27) and (28), require a considerably larger computation time than that of the other methods, especially when optimization of the aerodynamic lag values is performed [9]. A major reduction in the MS computation efforts may be obtained by applying approximation constraints.

B. Approximation constraints

It is often desired to apply approximation constraints in order to obtain exact fits at specified reduced frequencies or to null out some coefficients, even though the constraints increase the total fit errors. The most frequently used constraint is a match of the steady-aerodynamics data ($k = 0$). An imaginary-part data-match constraint at a k close to 0 yields the tabulated low-frequency quasi-steady aerodynamic damping. Data-match constraints at higher k values are sometimes desired to increase the accuracy of anticipated flutter mechanisms. The structural columns, $[A_{s_j}]$ of the apparent mass matrix, $[A_2]$, are sometimes set to 0 to avoid repetitive inversions of $[\bar{M}_s]$ of Eq. (7). The gust columns of $[A_2]$ are often set to $[A_{g_j}] = 0$, as discussed above Eq. (7). The option of nulling out terms in the aerodynamic damping matrix $[A_1]$ is also available but is usually not recommended.

Up to three linear equality constraints for each aerodynamic term can be used to explicitly determine $[A_0]$, $[A_1]$ and $[A_2]$, which reduces the approximation problem size. The three constraints are:

1. Steady aerodynamics match which yields

$$A_{0_{ij}} = F_{ij}(0) \tag{29}$$

2. A real-part match constraint at a nonzero $k = k_{f_{ij}}$ which yields

$$A_{2_{ij}} = \frac{1}{k_{f_{ij}}^2}\left(A_{0_{ij}} - F_{ij}(k_{f_{ij}})\right) + [D_i]\left(k_{f_{ij}}^2[I] + [R]^2\right)^{-1}\{E_j\} \quad (30)$$

which can be replaced by the $A_{2_{ij}} = 0$ constraint [13, 14], and

3. An imaginary-part match constraint at a nonzero $k = k_{g_{ij}}$ which yields

$$A_{1_{ij}} = \frac{1}{k_{g_{ij}}} G_{ij}(k_{g_{ij}}) + [D_i]\left(k_{g_{ij}}^2[I] + [R]^2\right)^{-1}[R]\{E_j\} \quad (31)$$

which can be replaced by the $A_{1_{ij}} = 0$ constraint.

The most drastic effect of using the constraints to reduce the approximation problem size is in the MS method. When the three data-match constraints of Eqs. (29)-(31) are applied simultaneously, and when all $k_{f_{ij}} = k_f$ and all $k_{g_{ij}} = k_g$, the MS $[D] \rightarrow [E] \rightarrow [D]$ least-square matrices, Eqs. (27) and (28), are replaced by

$$\begin{aligned} [A^*]_\ell &= \begin{bmatrix} k_\ell^2[D]\left[\left(k_\ell^2[I] + [R]^2\right)^{-1} - \left(k_f^2[I] + [R]^2\right)^{-1}\right] \\ -k_\ell[D]\left[\left(k_\ell^2[I] + [R]^2\right)^{-1} - \left(k_g^2[I] + [R]^2\right)^{-1}\right][R] \end{bmatrix}, \\ \{x^*\} &= \{E_j\}, \qquad \{b^*\}_\ell = \begin{Bmatrix} \bar{F}_j(k_\ell) \\ \bar{G}_j(k_\ell) \end{Bmatrix} \end{aligned} \quad (32)$$

and

$$\begin{aligned} [A^*]_\ell &= \begin{bmatrix} k_\ell^2[E]^T\left[\left(k_\ell^2[I] + [R]^2\right)^{-1} - \left(k_f^2[I] + [R]^2\right)^{-1}\right] \\ -k_\ell[E]^T\left[\left(k_\ell^2[I] + [R]^2\right)^{-1} - \left(k_g^2[I] + [R]^2\right)^{-1}\right][R] \end{bmatrix}, \\ \{x^*\} &= \{D_i^T\}, \qquad \{b^*\}_\ell = \begin{Bmatrix} \bar{F}_i^T(k_\ell) \\ \bar{G}_i^T(k_\ell) \end{Bmatrix} \end{aligned} \quad (33)$$

where the terms of $[\bar{F}]$ and $[\bar{G}]$ are

$$\begin{aligned} \bar{F}_{ij}(k_\ell) &= F_{ij}(k_\ell) - F_{ij}(0) - \left(F_{ij}(k_f) - F_{ij}(0)\right)\frac{k_\ell^2}{k_f^2} \\ \bar{G}_{ij}(k_\ell) &= G_{ij}(k_\ell) - G_{ij}(k_g)\frac{k_\ell}{k_g} \end{aligned} \quad (34)$$

The application of different constraint sets to different terms requires each row of $[A^*]_\ell$ and $\{b^*\}_\ell$ of Eqs. (32) and (33) to be calculated with a different

k_f or k_g. The applications of the $A_{1_{ij}} = 0$ and $A_{2_{ij}} = 0$ constraint options are performed by deleting the terms which include k_g and k_f respectively. With Eqs. (32) and (33), the number of unknowns in each application of Eq. (25) is reduced to n_L, which is typically about one seventh of that of the unconstrained problem.

A different way to enforce data match at $k \neq 0$ was presented in [9]. Instead of defining $[A_1]$ and $[A_2]$ explicitly, as in Eqs. (31) and (30), the data match was enforced by introducing Lagrange variables which increase the problem size. While this approach allowed a more flexible number of constraints, it made the computation time of an optimized MS application to a seven mode problem with one constraint to be more than 100 times that of the application of Roger's method. Since the number of aerodynamic lags, n_L, in the MS method is larger than in the other methods of similar accuracy, optimization of their values is more time consuming but not as important. A typical comparison between the applications of the MS and Roger's methods is given in [23] for a 10 mode case. An 8-lag MS approximation (which yields 8 aerodynamic states) with three constraints and without optimization was of the same level of fit accuracy as a 3-lag optimized Roger's approximation (which yielded 30 aerodynamic states) with one constraint (at $k = 0$). Based on the size and the number of least-square solutions in [23], it was argued that both applications required similar computational efforts.

VI. DATA WEIGHTING

The percentage deviations of uniformly weighted least-square curve fits from large data values are generally smaller than from small data values. This raises two problems in the context of aerodynamic approximations. One problem is that the approximation might be affected by the way the modes are normalized, even though the accurate solution is not. The other problem is that small aerodynamic data values are not necessarily less important than larger ones. The first problem can be resolved by a weighting that has the effect of data normalization (Subsection A). The physical weighting suggested in Subsection B resolves both problems.

A. Data Normalization

A way to avoid the effect of the manner in which structural modes are normalized is by defining the terms of the weight matrix $[W]_\ell$ as

$$W_{ij\ell} = \frac{\epsilon}{\max_\ell\{|Q_{ij}(ik_\ell)|, \epsilon\}} \quad (35)$$

where ϵ is a user-defined small positive parameter. The resulting absolute

value of a weighted aerodynamic term is

$$\bar{Q}_{ij}(k_\ell) = W_{ij\ell}|Q_{ij}(ik_\ell)| \tag{36}$$

The effect of this weighting is renormalization of the input data such that the maximum $|\bar{Q}(k_\ell)|$ of each ijth term is ϵ, with the exception that terms with maximum $|Q(ik_\ell)|$ of less than ϵ are not normalized. With $\epsilon = 1$, ε_t of Eq. (23) is consistent with the "common measure of approximation performance" in [9]. It should be noticed that the data-normalization $[W]_\ell$ matrices are the same for all ℓ values. Consequently, they have to be applied in the least-square solutions only when the unknowns appearing in a $\{x^*\}$ of Eq. (24) relate to different aerodynamic terms. Among the methods discussed above, this is the case only with the MS method. In the other methods, where the inner-loop approximations are performed term by term, these weights should be applied only to calculate ε_t by Eq. (23) for the evaluation of the approximation performance or for the optimization of the aerodynamic lag values.

B. Physical Weighting

The physical-weighting algorithm developed in [13-15] was designed to weight each term of the tabulated data such that the magnitude of the weighted term, Eq. (36), indicates its "aeroelastic importance". The idea is that the weight assigned to a data term should be proportional to the estimated effect of a unit approximation error on a representative aeroelastic property. Different representative properties are selected below for the structural, control and gust-related partitions of the AFC matrices. The error effects are estimated by the differentiation of the selected aeroelastic properties with respect to the aerodynamic terms. The weight calculations are performed with the frequency-domain coefficients of Eqs. (1) and (2) (with s replaced by $ik_\ell V/b$) which are already known at this stage of the modeling process for a nominal aeroservoelastic configuration. The weighting dynamic pressure is $q = q_d$ at which the open-loop system is stable.

The weights assigned to the terms of a structure-related AFC matrix $[Q_s(ik_\ell)]$ are based on their effect on the determinant of the system matrix $[C_s(ik_\ell)]$ of Eq. (1). The absolute values of the partial derivatives of this determinant of with respect to $Q_{s_{ij}}(ik_\ell)$, divided by the determinant itself, is shown in [13] to be the ijth term of the weight matrix

$$[\bar{W}_s]_\ell = q_d \left|[C_s(ik_\ell)]^{-1}\right|^T \tag{37}$$

The weights assigned to the terms in the jth column of a control-related AFC matrix $[Q_c(ik_\ell)]$ is based on the open-loop frequency response of the jth actuator to excitation by the jth control surface, derived from Eqs. (1) and (2). The magnitude of the partial derivative of this Nyquist signal with respect to $Q_{c_{ij}}(ik_\ell)$ is shown in [13] to be the ijth term of the weight matrix

$$[\bar{W}_c]_\ell = q_d \left|[T(ik_\ell)][\psi_m][C_s(ik_\ell)]^{-1}\right|^T \tag{38}$$

The physical-weighting transfer functions in $[T(ik_\ell)]$ should represent a basic control system. Structural, narrow-band filters with high sensitivity to parametric changes should not be included as it may result in the assignment of low weights to important aerodynamic data terms.

The weights assigned to the terms of the jth column of a gust-related AFC matrix $[Q_g(ik_\ell)]$ is based on the power spectral density (PSD) of the open-loop response of a selected structural acceleration to continuous gust, derived from Eq. (1),

$$\Phi_{z_j}(k_\ell) = \left|\frac{k_\ell^2 q_d V}{b^2}[\psi_{z_j}][C_s(ik_\ell)]^{-1}\{Q_{g_j}(ik_\ell)\}\right|^2 \Phi_{w_j}(k_\ell) \tag{39}$$

where $[\psi_{z_j}]$ is a row vector of modal displacements at the selected response point, and $\Phi_{w_j}(k)$ is the PSD function of the associated gust velocity. The partial derivative of $\sqrt{\Phi_{z_j}(k_\ell)}$ with respect to $Q_{g_{ij}}(ik_\ell)$ is the ijth term of the weight matrix

$$[\bar{W}_g]_\ell = \frac{k_\ell^2 q_d V}{b^2}\left|[\psi_z][C_s(ik_\ell)]^{-1}\right|^T [\bar{\Phi}_w]_\ell \tag{40}$$

where $[\bar{\Phi}_w]_\ell$ in an $n_g \times n_g$ diagonal matrix whose elements are $\sqrt{\bar{\Phi}_{w_j}(k_\ell)}$.

The variations of terms in the weight groups $[\bar{W}_s]_\ell$, Eq. (37), $[\bar{W}_c]_\ell$, Eq. (38), and $[\bar{W}_g]_\ell$, Eq. (40), with k may have very sharp peaks. In addition, the peak values of many terms may be several orders-of-magnitude smaller than other peaks. The extreme weight variations have the effect of neglecting much of the data, which may cause numerical ill-conditioning problems and unrealistic curve fits. To ensure realistic interpolation between the tabulated k values, and to facilitate the application of the resulting aeroelastic model to a variety of flow conditions, structural modifications, and control parameters, it may be desirable to moderate the weight variations. This is performed by widening the weight peaks and by scaling up the extremely low weights. The peak widening is performed in n_{wd} cycles where, in each cycle, $\bar{W}_{ij}(k_\ell)$ is changed to $\max\{\bar{W}_{ij}(k_{\ell-1}), \bar{W}_{ij}(k_\ell), \bar{W}_{ij}(k_{\ell+1})\}$ of the previous cycle. The weight matrices are then normalized and combined to the final weight matrix

$$[W]_\ell = \left[\ [W_s]_\ell \quad [W_c]_\ell \quad [W_g]_\ell \ \right] \tag{41}$$

where a term in $[W_s]_\ell$ is

$$W_{s_{ij\ell}} = \left(\max\left\{\frac{1}{\max_{i,j}\{\bar{W}_{s_{ij}}\}}, \frac{W_{cut}}{\bar{W}_{s_{ij}}}\right\}\right)\bar{W}_{s_{ij\ell}} \tag{42}$$

where

$$\bar{W}_{s_{ij}} = \max_{\ell} \{|Q_{s_{ij}}(ik_\ell)|\bar{W}_{s_{ij\ell}}\}$$

and the terms of $[W_c]_\ell$ and $[W_g]_\ell$ are calculated similarly (but separately). The upscale parameter W_{cut} is defined by the analyst. The resulting magnitudes of the weighted terms, $\bar{Q}_{ij}(k_\ell)$ of Eq. (36), fall between W_{cut} and 1.0 when the value of 1.0 typically appears only once in each group. The modified physical weighting is actually a compromise between the the unmodified one (with n_{wd} and W_{cut} equal zero) and the data-normalization weighting, Eq. (35). With $n_{wd} \doteq n_h$ and $W_{cut} = 1.0$, all the physical-weighting effects are suppressed and the weighting becomes a data-normalization one. Recommended parameters in typical cases [14] are $n_{wd} = 2$ and $W_{cut} = 0.01$. Various applications demonstrated that the resulting aeroservoelastic models were adequate for analyses with large variations of dynamic pressures [13-16], control gains [8], and structural parameters [24].

C. Modal Measures of Aeroelastic Importance

The physical weights can be used to rate the vibration modes according to their relative aeroelastic importance. Based on the magnitudes of the weighted aerodynamic data terms, Eq. (36), calculated with n_{wd} and W_{cut} equal zero, three modal measures of aeroelastic importance are defined for each structural vibration mode by

$$\begin{aligned} Q^*_{s_i} &= \max_{j,\ell} \{|\bar{Q}_{s_{ij}}(ik_\ell)|\}, \qquad Q^*_{c_i} = \max_{j,\ell} \{|\bar{Q}_{c_{ij}}(ik_\ell)|\}, \\ Q^*_{g_i} &= \max_{j,\ell} \{|\bar{Q}_{g_{ij}}(ik_\ell)|\} \end{aligned} \tag{43}$$

These measures can be interpreted as indicators of the aeroelastic activity of the ith vibration mode, on a scale of 0 to 1, in three categories: a) influence on the open-loop system roots (Q^*_s); b) role in the aeroservoelastic loop (Q^*_c); and c) contribution to gust response (Q^*_g). Being based on a limited analysis, these measures should be used with caution. Their main usage is in supplying physical insight and in pointing out the structural modes that can be eliminated from the model without causing significant errors.

VII. RESIDUALIZATION OF STRUCTURAL STATES

A. General

It is assumed at this point that an aeroservoelastic model, Eqs. (11) and (12), has already been established with an initial set of vibration modes

and that it is now desired to reduce the model size by eliminating structural states which have a negligible effect on the model accuracy. The modes to be eliminated are identified by either performing a preliminary analysis or by inspecting the modal measures of aeroelastic importance discussed in Section VI-C above. The state vector $\{x\}$ is partitioned into two subsets, $\{x_r\}$ and $\{x_e\}$, where $\{x_e\}$ is to be constrained and eliminated from the state vector, and $\{x_r\}$ is to be retained. In our case, $\{x_e\}$ includes only the structural states $\{\xi_e\}$ and $\{\dot{\xi}_e\}$ which represent the eliminated vibration modes. The formulation in this section follows that of [20]. The main differences stem from the fact that the gust filter in this work, Eq. (9), does not include a noise term in its output.

The partitioning of Eqs. (11) and (12) into $\{x_r\}$ and $\{x_e\}$ related partitions yields

$$\begin{bmatrix} Z_{rr} & Z_{re} \\ Z_{er} & Z_{ee} \end{bmatrix} \begin{Bmatrix} \dot{x}_r \\ \dot{x}_e \end{Bmatrix} = \begin{bmatrix} A_{rr} & A_{re} \\ A_{er} & A_{ee} \end{bmatrix} \begin{Bmatrix} x_r \\ x_e \end{Bmatrix} + \begin{bmatrix} B_r \\ 0 \end{bmatrix} \{u\} + \begin{Bmatrix} B_{w_r} \\ 0 \end{Bmatrix} w \tag{44}$$

and

$$\{y\} = \begin{bmatrix} C_r & C_e \end{bmatrix} \begin{Bmatrix} x_r \\ x_e \end{Bmatrix} \tag{45}$$

With the assumption that the effects of $\{\dot{x}_e\}$ on the top partition of Eq. (44) may be neglected, the most general constraints which allow model size reduction are

$$\{x_e\} = [F]\{x_r\} + [G]\{u\} + \{G_w\}w + [H]\{\dot{x}_r\} \tag{46}$$

The coefficient matrices in Eq. (46) are defined in the following subsections for the various size-reduction methods. It should be mentioned that Eq. (46) does not necessarily define the motion of the eliminated modes. It only defines the portion of this motion that affects the remaining model. The substitution of Eq. (46) into the top partition of Eq. (44) with $[Z_{re}]\{\dot{x}_e\} = 0$ yields the residualized equation of motion

$$\left[\tilde{Z}\right]\{\dot{x}_r\} = [\tilde{A}]\{x_r\} + [\tilde{B}]\{u\} + \{\tilde{B}_w\}w \tag{47}$$

and the associated output equation

$$\{y\} = [\tilde{C}]\{x_r\} + [\tilde{D}]\{u\} + \{\tilde{D}_w\}w \tag{48}$$

where the matrix coefficients are

$$\left[\tilde{Z}\right] = [Z_{rr}] - [A_{re}][H], \qquad \left[\tilde{A}\right] = [A_{rr}] + [A_{re}][F],$$

$$
\begin{aligned}
\left[\tilde{B}\right] &= [B_r] + [A_{re}][G], \qquad \left\{\tilde{B}_w\right\} = \{B_{w_r}\} + [A_{re}]\{g_w\}, \\
\left[\tilde{C}\right] &= [C_r] + [C_e]\left([F] + [H][\tilde{Z}]^{-1}[\tilde{A}]\right), \\
\left[\tilde{D}\right] &= [C_e]\left([G] + [H][\tilde{Z}]^{-1}[\tilde{B}]\right), \\
\left\{\tilde{D}_w\right\} &= [C_e]\left(\{G_w\} + [H][\tilde{Z}]^{-1}\{\tilde{B}_w\}\right)
\end{aligned} \tag{49}
$$

B. Mode Truncation

The simplest and most commonly used size-reduction technique is based on the assumption that the eliminated states have no effects on the dynamics and on the output of the system, namely the coefficient matrices of Eq. (46) are all zero. The resulting model is that of Eqs. (44) and (45) where all the rows and columns associated with $\{x_e\}$ are truncated.

C. Static Residualization

Static residualization is based on the principles of static aeroelastic analysis using vibration modes (such as in [19]) where the aerodynamics associated with the deflections of the elastic modes have a major impact on the rigid-body aerodynamics. In the present application it is assumed that the $\{\xi_e\}$ effects are important but the $\{\dot{\xi}_e\}$ and $\{\ddot{\xi}_e\}$ effects may be neglected. With these assumptions, the bottom row partition of Eq. (44) and the matrix definitions of Eq. (10) yield

$$
[\bar{K}_{ee}]\{\xi_e\} = [F_1]\{x_r\} - [\bar{M}_{er}]\{\ddot{\xi}_r\} \tag{50}
$$

where

$$
[F_1] = -\begin{bmatrix} \bar{K}_{ee} & \bar{B}_{er} & \bar{D}_e & \bar{F}_{c_e} & \bar{F}_{g_e} \end{bmatrix}
$$

Equation (50) and $\{\dot{\xi}_e\} = 0$ yield the constraint matrices of Eq. (46) for the case of static residualization

$$
\begin{aligned}
[F] &= \begin{bmatrix} \bar{K}_{ee}^{-1} \\ 0 \end{bmatrix}[F_1], \qquad [G] = [0], \qquad \{G_w\} = \{0\}, \\
[H] &= -\begin{bmatrix} \bar{K}_{ee}^{-1} \\ 0 \end{bmatrix}\begin{bmatrix} 0 & \bar{M}_{er} & 0 & 0 & 0 \end{bmatrix}
\end{aligned} \tag{51}
$$

The statically residualized model of Eqs. (47) and (48) can now be constructed using Eqs. (49) and (51). It can be shown from Eqs. (10), (49), and (51) that the matrix coefficients of the resulting state-space equation

have the same topology (non-zero partitions) as those of the full-size equation (10), and that the output equation remains with no control and noise terms, namely $[\tilde{D}] = 0$ and $\{\tilde{D}_w\} = 0$.

D. Dynamic Residualization

The dynamic residualization suggested in [20] does not neglect apriori the effects of $\{\dot{\xi}_e\}$. The extension of Eq. (50), using Eq. (10), to include these effects reads

$$
[\bar{K}_{ee}]\{\xi_e\} = [F_1]\{x_r\} - [\bar{M}_{er}]\{\ddot{\xi}_r\} - [\bar{B}_{ee}]\{\dot{\xi}_e\} \tag{52}
$$

where the first term on the right side is the primary contributor to the generalized forces acting on the eliminated modes and the other terms have secondary effects. The differentiation of Eq. (52) with respect to time, while neglecting the derivatives of the secondary effects and using the definition of $[F_1]$ in Eq. (50), yields an equation for $\{\dot{\xi}_e\}$:

$$
[\bar{K}_{ee}]\{\dot{\xi}_e\} = -[\bar{K}_{er}]\{\dot{\xi}_r\} - [\bar{B}_{er}]\{\ddot{\xi}_r\} - [\bar{D}_e]\{\dot{x}_a\} - [\bar{F}_{c_e}]\{\dot{x}_c\} - [\bar{F}_{g_e}]\{\dot{x}_g\} \tag{53}
$$

which, by using Eq. (10) for $\{\dot{x}_a\}$, $\{\dot{x}_c\}$, and $\{\dot{x}_g\}$, becomes

$$
[X_{22}]\{\dot{\xi}_e\} = [F_2]\{x_r\} - [\bar{F}_{c_e}][B_c]\{u\} - [\bar{F}_{g_e}]\{B_g\}w - [\bar{B}_{er}]\{\ddot{\xi}_r\} \tag{54}
$$

where

$$
\begin{aligned}
[X_{22}] &= [\bar{K}_{ee}] + [\bar{D}_e][E_{ee}] \\
[F_2] &= -\begin{bmatrix} 0 & \bar{K}_{er} + \bar{D}_e E_{er} & \bar{D}_e\bar{R} & \bar{D}_e\hat{E}_c + \bar{F}_{c_e}A_c & \bar{D}_e\hat{E}_g + \bar{F}_{g_e}A_g \end{bmatrix}
\end{aligned}
$$

Equations (52) and (54) yield the constraint matrices of Eq. (46) for the case of dynamic residualization

$$
\begin{aligned}
[F] &= [X]^{-1}\begin{bmatrix} F_1 \\ F_2 \end{bmatrix}, \qquad [G] = -[X]^{-1}\begin{bmatrix} 0 \\ \bar{F}_{c_e}B_c \end{bmatrix}, \\
\{G_w\} &= -[X]^{-1}\begin{Bmatrix} 0 \\ \bar{F}_{g_e}B_g \end{Bmatrix}, \\
[H] &= -[X]^{-1}\begin{bmatrix} 0 & \bar{M}_{er} & 0 & 0 & 0 \\ & \bar{B}_{er} & & & \end{bmatrix}
\end{aligned} \tag{55}
$$

where

$$
[X]^{-1} = \begin{bmatrix} \bar{K}_{ee}^{-1} & -\bar{K}_{ee}^{-1}\bar{B}_{ee}X_{22}^{-1} \\ 0 & X_{22}^{-1} \end{bmatrix}
$$

The dynamically residualised model of Eqs. (47) and (48) can now be constructed using Eqs. (49) and (55). It can be shown from Eqs. (10), (49) and (55) that $[\tilde{Z}]$ of Eq. (47) still has the same topology as $[Z_{rr}]$. However, unlike the static residualization, the topology of $[\tilde{A}]$, $[\tilde{B}]$, and $\{\tilde{B}_w\}$ resulting from the dynamic residualization does not keep the original topology. In addition, $[\tilde{D}]$ and $\{\tilde{D}_w\}$ are not equal zero. It should be noted that setting $\{G_w\} = 0$ instead of $\{G_w\}$ of Eq. (55), which is usually an adequate assumption, would null out $\{\tilde{D}_w\}$ such that there would not be a noise term in the output equation. The added terms in Eq. (48) modify the closed-loop equation, Eq. (15), which becomes

$$\left[\tilde{Z}\right]\{\dot{x}_r\} = [\hat{A}]\{x_r\} + \{\hat{B}_w\}w \tag{56}$$

where

$$\begin{aligned}\left[\hat{A}\right] &= [\tilde{A}] + [\tilde{B}]\left([I] - [G_c][\tilde{D}]\right)^{-1}[G_c][\tilde{C}] \\ \left\{\hat{B}_w\right\} &= \{\tilde{B}_w\} + [\tilde{B}]\left([I] - [G_c][\tilde{D}]\right)^{-1}[G_c]\{\tilde{D}_w\}\end{aligned}$$

The columns of $[A_2]$ of Eq. (4) which relate to the eliminated modes are neglected in all the size-reduction techniques discussed in this section. Constraining them to be zero in the aerodynamic approximation process may improve the accuracy of the reduced-size model. The use of dynamically residualised models in aeroservoelastic optimisation is discussed in [25].

VIII. NUMERICAL EXAMPLE

A. The Mathematical Model

The numerical application deals with the mathematical model of NASA's Drone for Aerodynamic and Structural Testing - Aerodynamic Research Wing 1 (DAST-ASW1) [5]. A top view of the model geometry is given in Fig. 1. The same model was also used by Nissim [18] to demonstrate his aerodynamic approximation method in comparison with Roger's method. The main results of [18] are compared in this section to flutter characteristics derived from aeroservoelastic models which are based on the Minimum-State (MS) approximation method.

The model consists on ten symmetric natural vibration modes and one trailing-edge control-surface mode. The oscillatory AFC matrices were calculated using doublet lattice aerodynamics [3] at Mach 0.9. The control surface is driven by a third-order actuator whose transfer function is

$$\frac{\delta}{\delta_c} = \frac{1.915 \times 10^7}{(s+214)(s^2+179.4s+89450)} \tag{57}$$

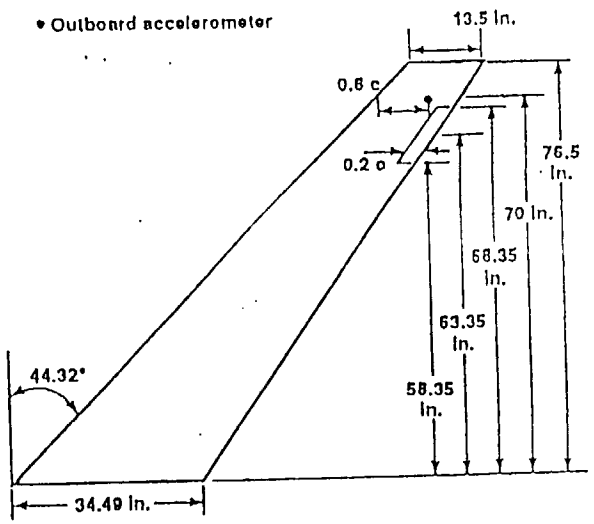

Fig. 1. Model geometry of DAST-ARW1.

Closed-loop results will be shown for two control laws which relate the actuator input, δ_c, to the acceleration, $\ddot{h}_{outb}$, measured by an outboard accelerometer (Fig. 1). The transfer function of the first control law (CL1), developed in [5], is

$$\frac{\delta_c}{\ddot{h}_{outb}} = \frac{0.1}{(s+10)}\frac{s}{(s+1)}\frac{628.3^2}{(s+628.3)^2}\left[\frac{s^2+30.79s+14692}{s^2+572.6s+88578}\right] \times \left[\frac{s^2+47.37s+72436}{s^2+568.6s+86972}\right]\frac{rad}{in/sec^2} \tag{58}$$

The transfer function of the second control law (CL2), developed in [26], is

$$\frac{\delta_c}{\ddot{h}_{outb}} = 5.745 \times 10^{-6}\left[\frac{s+185.8}{s+630}\right]\left[\frac{s^2+155s+29658}{s^2+13.53s+272.25}\right]\frac{rad}{in/sec^2} \tag{59}$$

The dynamics of the accelerometer are neglected. The total control transfer function is obtained by multiplying CL1 or CL2 by the actuator transfer function, Eq. (57). The realization of the control system in state-space form, Eq. (8), yields 11 control states for CL1 and 6 for CL2.

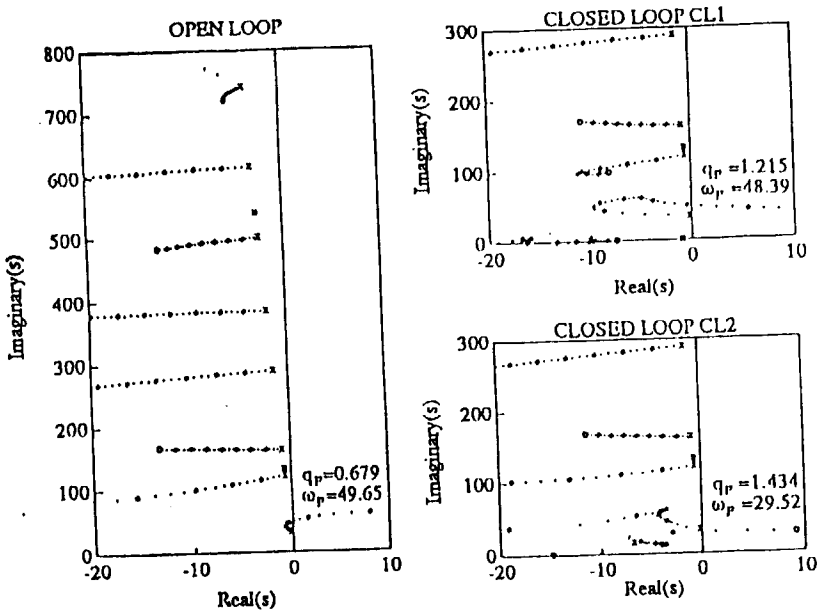

Fig. 2. Open and closed-loop root loci of DAST-ARW1.

B. Flutter Results with Various Aerodynamic Approximations

The results shown in this subsection are based on the same aerodynamic data used in [18]. This data, which will be referred to as Data 1, consists on 10 AFC matrices calculated at $k_\ell = 0.$, 0.05, 0.1, 0.2, 0.3, 0.4, 0.5, 0.6, 0.7, and 0.8. The reference "true" results are those obtained with Roger's method with 4 aerodynamic lag terms, $\gamma_l = 0.1$, 0.2, 0.3, and 0.4. These lags were used in all the analyses of this subsection. When the number of lags is less than four, the first ones are taken. The generalized structural damping matrix, $[B_s]$ of Eq. (1), is assumed to be

$$[B_s] = 2\zeta[M_s][\omega_n] \tag{60}$$

where $[\omega_n]$ is a diagonal matrix of natural frequencies, and ζ is the modal damping coefficient, 0.01 in this work. The open- and closed-loop flutter conditions were found by root-locus analysis of the respective system matrix with variable dynamic pressure (q). Typical root-loci plots, where q varies in constant increments from 0 to 1.6 psi (marked by X and O respectively) are shown if Fig. 2. It can be observed that all the flutter mechanisms are of low frequency but there are significant differences between the flutter conditions of the three cases. The high-frequency closed-loop branches (not shown) are almost identical to the open-loop ones.

The MS modeling method was applied to Data 1 with 4 aerodynamic lags and with three data-match constraints, one at $k = 0$ and two at k_f =0.8, assigned to each aerodynamic term. The least-square solution was performed in 50 $[D] \rightarrow [E] \rightarrow [D]$ iterations with the physical weighting of Section VI-B, performed at $q_d = 0.5$ psi and modified with n_{wd}=2 and W_{cut}=0.01. These typical parameters are based on the experience gained in previous applications of the MS method [13-16]. The trunster function used to calculate the control-column weights, Eq. (38), was that of the actuator only. The open and closed-loop flutter results are compared in Table 1 to some of those given in [18] for Roger's and Nissim's methods.

Method	n_L	Modes with lags	n_a	q_f (psi)	ω_f rad/s	ε_q (%)	ε_ω (%)
Open-loop							
Roger	4	All	40	0.677	49.6	0.0	0.0
Roger	2	All	20			-0.3	-0.2
Roger	1	All	10			0.2	-0.2
Nissim	1	1,2	2			0.1	-0.2
MS	4	All	4	0.679	49.7	0.3	0.2
Closed-loop CL1							
Roger	4	All	40	1.215	48.4	0.0	0.0
Roger	2	All	20			-0.1	-0.2
Roger	1	All	10			2.6	0.6
Nissim	1	1,2	2			-3.9	5.1
Nissim	1	1,2,4,5	4			3.7	-0.4
Nissim	2	1,2	4			-5.9	5.1
Nissim	2	1,2,4,5	8			-0.3	-1.0
MS	4	All	4	1.197	49.7	-1.5	2.6
Closed-loop CL2							
Roger	4	All	40	1.426	29.4	0.0	0.0
Roger	2	All	20			-1.0	2.7
Roger	1	All	10			1.6	-3.7
Nissim	1	1,2	2			0.7	3.7
MS	4	All	4	1.435	29.8	0.6	1.4

Table 1. Comparison of flutter results with various modeling methods.

Due to a slight difference between the definitions of structural damping, the true flutter results in this work, q_F and ω_F, are slightly different than those of [18]. It is assumed, however, that the differences has no effect on the flutter percentage errors, ϵ_q and ϵ_ω. It can be observed that, in this example, the MS and Nissim's methods yield similar numbers of aerodynamic states (n_a) per desired accuracy. It should be noted, however, that while the presented Nissim's results were obtained after a careful selection of the best lag values and the modes to which they should be applied, the MS modeling did not require such an investigation.

C. Effects of Data Points and Approximation Constrains

Since flutter is more likely to involve the low-frequency modes than the high-frequency ones, the common practice is to include in the tabulate data more AFC matrices in the low-frequency range than in the higher one. To conform with this approach, and to investigate the effects of various data-match constraints, a new aerodynamic data set, refered to as Data 2, was generated. The new data consists on 11 AFC matrices at k_ℓ = 0., 0.02, 0.0544, 0.07, 0.0896, 0.11, 0.15, 0.2, 0.3, 0.5 and 0.8. The 0.0544 and 0.0896 valued were chosen because they are the true flutter reduced frequency values, k_F, of the closed-loop cases CL2 and CL1 respectively. The open-loop true k_F is 0.0919.

Data 2 was used to construct MS models with the same physical weighting parameters as above, but with three different constraint sets, one with all the aerodynamic terms constrained to match the data at k_ℓ = 0.8 (as in the Data 1 case), one with k_ℓ = 0.0896, and one with k_ℓ = 0.0544. In addition, all the approximations were constrained to match the data at k =0. A comparison of the resulting flutter errors is given in Table 2. The comparison between the first two cases shows that the larger amount of low-frequency data in Data 2 resulted in smaller errors than with Data 1. A further error reduction is obtained when the data-match constraints are at k values which are closer to k_F.

		Open-loop		Closed-loop CL1		Closed-loop CL2	
Data	k_ℓ	ϵ_q	ϵ_ω	ϵ_q	ϵ_ω	ϵ_q	ϵ_ω
1	0.8	0.28	0.16	-1.48	2.60	0.63	1.36
2	0.8	0.31	0.22	-0.99	1.94	0.56	0.78
2	0.0896	0.03	0.02	0.00	0.00	0.35	-0.61
2	0.0544	-0.18	-0.06	-0.66	-0.27	0.00	0.00

Table 2. Effects of data points and constraints on percentage flutter errors.

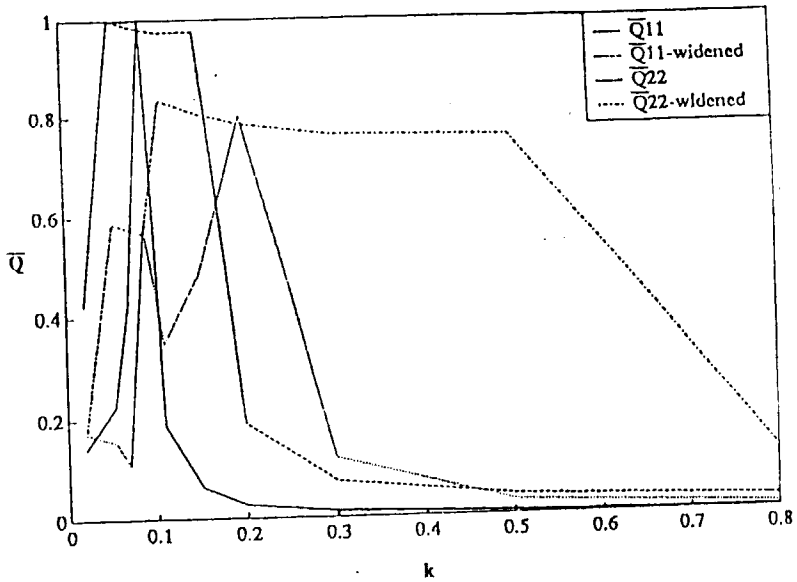

Fig. 3. Magnitudes of weighted aerodynamic terms versus reduced frequency.

It should be remembered that a major reason for applying the constraints when using the MS method is that they reduce the problem size. In our numerical example, in each of the 50 least-square iterations there are two inversions of 4x4 matrices. Without the constraints, the inversions in each iteration would have been one of a 34x34 matrix and one of a 37x37 matrix. Even though the application of data-match constraints at the highest k_ℓ value yielded the largest flutter error, it had the least effect on the total approximation error (not shown).

D. The Physical Weights

When the physical weighting is performed with n_{wd} =0 and W_{cut} =0, the magnitudes of the aerodynamic data terms, $\bar{Q}_{ij}(k_\ell)$ of Eq. (36), indicate their aeroelastic importance. Typical variations of $\bar{Q}_{ij}$ values of important terms, calculated with Data 2, versus k are shown in Fig. 3. It can be observed that $\bar{Q}_{11}$ has a sharp peak which may cause the approximation to deteriorate at off-peak values. The variations of the same terms, but with the peaks widened in two widening cycles (n_{wd} =2), are also shown. With the modified weights, good least-square fits are expected over a wider

range of reduced frequencies, which makes the accuracy of the resulting model less sensitive to parametric changes.

The largest $\bar{Q}$ values, calculated separately for each aerodynamic term and rounded to the third decimal place, are given in Table 3. The rows and columns associated with modes 3 and 8 are not shown because all their values are rounded to zero. The maximal value in each row among the ten structural columns, and the associated value at the control column are the modal measures of aeroelastic importance, $Q^*_{s_i}$ and $Q^*_{c_i}$ of Eq. (43) Table 3 indicates that modes 1, 2, 4 and 5 are the most important (in decreasing order of importance). This is in agreement with the modes to which aerodynamic lags are applied in the Nissim's method cases of Table 1, and with the aeroelastic behavior of the modes in Fig. 2. Eighty percent of the structural $\bar{Q}_{max}$ values of Table 3, and fifty percent of the control $\bar{Q}_{max}$ values, are less that 0.01. With W_{cut} =0.01, the weights assigned to these terms are upscaled such that their $\bar{Q}_{max}$ =0.01.

Minimum-State approximations of Data 2 were performed with the number of aerodynamic lags, n_L, varying from 2 to 10. The n_L diagonal values of $[R]$ where arbitrarily chosen between -0.05 and -1.5 with more values close to -0.05 than to -1.5. Two models were constructed for each n_L case, one with the physical weighting used to construct the model of the second case in Table 2, and one with data-normalization weighting. The RMS values of the resulting errors in flutter dynamic pressure and flutter frequency of the three open and closed-loop cases together are shown in Fig. 4. These results are in agreement with those of [13-16] that showed that the number of aerodynamic states required for a certain level of model accuracy when physical weighting is used is about 50% of that required when physical weighting is not used.

	j=1	j=2	j=4	j=5	j=6	j=7	j=9	j=10	j=11
i=1	1.000	.595	.038	.014	.000	.001	.000	.000	1.000
i=2	.593	.800	.049	.025	.001	.002	.000	.000	.355
i=4	.047	.051	.344	.021	.002	.000	.000	.000	.081
i=5	.029	.016	.020	.321	.005	.001	.000	.000	.039
i=6	.001	.001	.002	.005	.048	.001	.000	.000	.013
i=7	.001	.001	.000	.001	.001	.029	.000	.000	.002
i=9	.000	.000	.000	.000	.000	.000	.011	.000	.000
i=10	.000	.000	.000	.000	.000	.000	.000	.003	.000

Table 3. Maximum magnitudes of weighted aerodynamic terms.

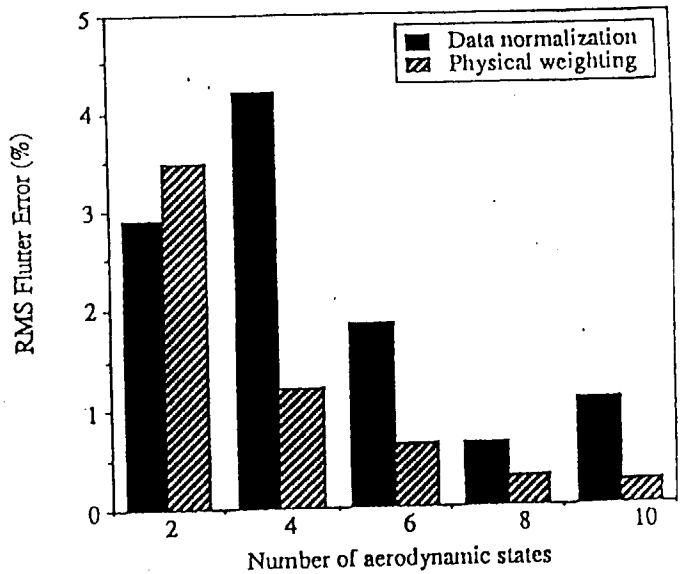

Fig. 4. Minimum-State flutter errors versus number of aerodynamic states.

E. Convergence in the Minimum-State Procedure

All the MS approximations of Fig. 4 were performed with 50 $[D] \rightarrow [E] \rightarrow [D]$ least-square iterations. The variations of the total approximation error, ε_t of Eq. (23), with the number of iterations are shown in Fig. 5. Because the data-normalization (N) weights, Eq. (35) with ϵ =1, are very different than the physical weights (PW), the errors of the two cases are not comparable. The relative effects of adding an approximation root in each of the two cases are similar. Since most of the weights in the PW cases are very small, ther is effectively less data to fit than in the N cases. Consequently, the PW cases converge faster and more consistently. Most error reductions are in the first few iterations. While the error in each case is reduced monotonously, the convergence rate may not, which may cause numerical difficulties when a convergence criteria is applied or when optimization of the lag values is attempted.

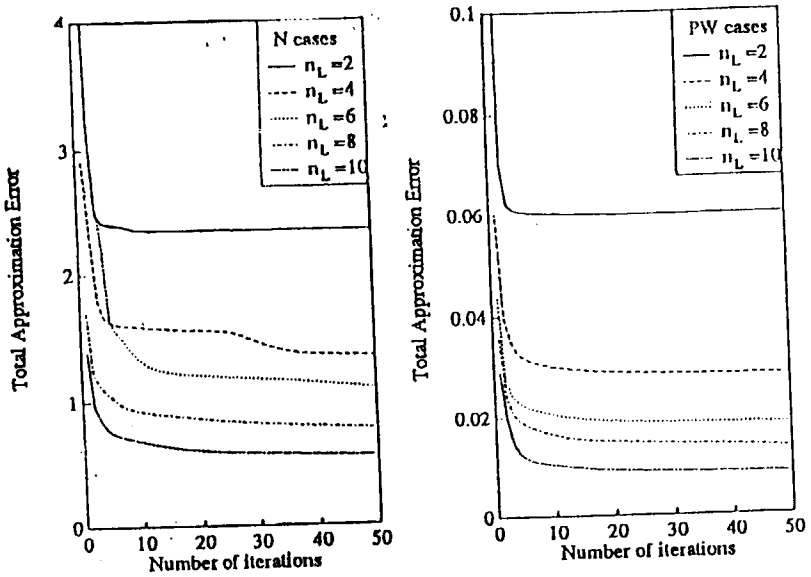

Fig. 5. Approximation errors versus number of Minimum-State iterations.

F. Elimination of Structural States

As shown above, high-accuracy aeroservoelastic models can be constructed for our application with only four aerodynamic states. A "full-size" 10-mode model has 20 structural states, the largest among the structural, aerodynamic and control state groups. Hence, a major improvement of the model efficiency can be achieved when some of the structural states are eliminated.

The third case of Table 2 was used as a baseline for the investigation of the effect of eliminating structural states. As mentioned before, the measures of aeroelastic importance given in Table 3 indicate that modes 1 and 2 are the most important and that modes 3 and 8 are the least important. Figure 6 shows the effects of mode truncation, and static and dynamic residualizations on the RMS errors in q_F and ω_F, calculated separately for the open-loop and the two closed-loop cases. Modes 3 and 8 were truncated in all the cases. Other modes were then truncated one by one, in decreasing frequency order. Figure 6 shows that up to 4 modes (8 states) can be truncated without any visible impact on the accuracy. The errors are still less than 1% with the truncation of 6 modes, but with the truncation of more modes, the errors grow to unacceptable levels where the largest errors are in the open-loop flutter dynamic pressure, more than 100%. With static and dynamic residualizations, 8 modes can be eliminated with RMS error levels of less than 3% and 1% respectively. The open-loop model in this case has only 8 states (4 structural and 4 aerodynamic). The CL1 and CL2 models have additional states, 11 and 6 respectively.

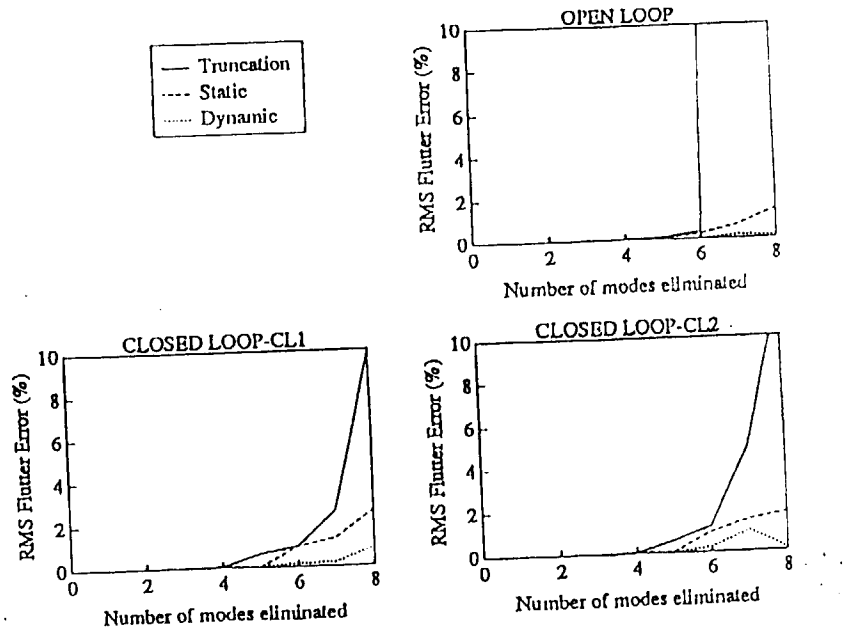

Fig. 6. Percentage RMS flutter errors versus number of eliminated modes.

IX. CONCLUSIONS

Size-reduction techniques for the determination of efficient time-domain, state-space aeroservoelastic models were presented. Various rational function approximation methods of the unsteady aerodynamic force coefficients were brought to a common notation, which emphasizes their differences. Among those, the classic Roger's method is the easiest to apply but its resulting number of aerodynamic states is typically equal to or larger than

the number of structural states. On the other side of the spectrum is the Minimum-State method which typically reduces the number of aerodynamic states by 70% or more, but requires the solution of an iterative, nonlinear least-square solution. The Minimum-State computational efforts are reduced significantly when three approximation constraints are applied. These constrained can be used to improve the fit at a desired reduced frequency. A selective application of Roger's formula, where aerodynamic lags are assigned only to a small number of modes, may also result in small-size models, but only in cases where the aeroelastic behavior is dominated by a small number of modes, and these modes are known apriori. The presented physical weighting of the aerodynamic data yields a further reduction (about 50%) in the number of states per desired accuracy. The physical weights can also be used to rate the structural modes according to their relative aeroelastic importance. The elimination of structural states associated with the less important modes by performing dynamic residualization was shown to be considerably more accurate than mode truncation and static residualization.

ACKNOWLEDGMENT

This research was supported by NASA Grant NAGW-1708. This support is gratefully acknowledged.

REFERENCES

1. R. L. Bisplinghoff, H. Ashley, and R. L. Halfman, "Aeroelasticity," Addison-Weseley, Cambridge, Mass., 1955.
2. R.L. Bisplinghoff and H. Ashley, "Principles of Aeroelasticity," Wiley, New York, 1962.
3. E. Albano and W. P. Rodden, "A Doublet-Lattice Method for Calculating Lifting Disturbances of Oscillating Surfaces in Subsonic Flow", *AIAA J.* **7**(2), 279-285 (1969).
4. W. M. Adams Jr., S. H. Tiffany, J. R. Newsom and E. L. Peele, "STABCAR - A Program for Finding Characteristic Roots of Systems Having Transcendental Stability Matrices", **NASA TP-2165** (1984).
5. J. R. Newsom, I. Able and H. J. Dunn, "Application of Two Design Methods for Active Flutter Suppression and Wind-Tunnel Test Results", **NASA TP-1653** (1980).
6. V. Mukhopadhyay, J. R. Newsome and I. Abel, "A Method for Obtaining Reduced-Order Control Laws for High-Order Systems Using Optimization Techniques," **NASA TP-1876** (1981).
7. P. D. Arbuckle, C. S. Buttrill, and T. A. Zeiler, "A New Simulation Model Building Process for use in Dynamics Systems Integration Research", *Proc. AIAA Flight Simulation Technologies Conf., Monterey, Ca* (1987).
8. M. Karpel, "Sensitivity Derivatives of Flutter Characteristics and Stability Margins for Aeroservoelastic Design", *J. Aircraft*, **27**(4), 368-375 (1990).
9. S. H. Tiffany and W. M. Adams Jr., "Nonlinear Programming Extensions to Rotational Approximation Methods of Unsteady Aerodynamic Forces", **NASA TP-2776** (1988).
10. K. L. Roger, "Airplane Math Modeling and Active Aeroelastic Control Design," **AGARD-CP-228**, 4.1-4.11 (1977).
11. M. Karpel, "Design for Active and Passive Flutter Suppression and Gust Alleviation", **NASA CR-3482** (1981)
12. M. Karpel, "Design for Active Flutter Suppression and Gust Alleviation Using State-Space Aeroelastic Modeling", *J. Aircraft*, **19**(3), 221-227 (1982).
13. M. Karpel, "Time-Domain Aeroservoelastic Modeling Using Weighted Unsteady Aerodynamic Forces", *J. Guidance, Control, and Dyn.*, **13**(1), 30-37 (1990).
14. M. Karpel, "Extension to the Minimum-State Aeroelastic Modeling Method", *AIAA J.*, **29**(11), 2007-2009 (1991).
15. M. Karpel and S. T. Hoadley, "Physically Weighted Approximations of Unsteady Aerodynamic Forces Using the Minimum-State Method", **NASA TP-3025** (1991).
16. S. T. Hoadley and M. Karpel, "Application of Aeroservoelastic Modeling Using Minimum-State Unsteady Aerodynamic Approximations", *J. Guidance, Control, and Dyn.*, **14**(6), 1267-1276 (1991).
17. E. Nissim and I. Lottati, "An Optimization Method for the Determination of the Important Flutter Modes",*J. Aircraft*, **18**(8), 663-668 (1981).
18. E. Nissim, "Reduction of Aerodynamic Augmented States in Active Flutter Suppression Systems," *J. Aircraft*, **28**(1), 82-93, (1991).
19. Z. Sheena and M. Karpel, "Static Aeroelastic Analysis Using Aircraft Vibration Modes", *Coll. Papers Second Int. Symp. Aeroelasticity and Struct. Dyn.*, Aachen, Germany, 229-232 (1985).
20. M. Karpel, "Reduced-Order Aeroelastic Models via Dynamic residualization", *J. Aircraft*, **27**(5), 449-455 (1990).
21. H. J. Hassig, "An Approximate True Damping Solution of the Flutter Equation by Determinant Iteration," *J. Aircraft*, **8**(11), 885-889 (1971).

22. W. Eversman and A. Tewari, "Consistent Rational-Function Approximation for Unsteady Aerodynamics," *J. Aircraft*, **28**(9), 545-552 (1991).
23. M. Karpel, "Reduced Size First-Order Subsonic and Supersonic Aeroelastic Modeling", *Proc. AIAA/ASME/ASCE/AHS 31st Struct., Str. Dyn. and Materials Conf.*, Long Beach, Ca, 1405-1417 (1990).
24. M. Karpel and C. D. Wieseman "Modal Coordinates for Aeroelastic Analysis with Large Local Structural Variations", *Proc. Int. Forum on Aeroelasticity and Struct. Dyn. 1991*, Aachen, Germany, 364-370 (1991).
25. I. Herssberg and M. Karpel, "Sensitivity Derivatives for Residualized Aeroservoelastic Optimum Design Models", *Proc. Int. Forum on Aeroelasticity and Struct. Dyn. 1991*, Aachen, Germany, 371-378 (1991).
26. E. Nissim, "Design of Control Laws for Flutter Suppression Based on the Aerodynamic Energy Concept and Comparisons With Other Design Methods", **NASA TP-3056** (1990).